Dual band Orthogonal Polarized 2-port MIMO Antenna for Cognitive Radio Applications

Shubhalaxmi Mohapatra[1], Satyadeep Das[1], Jyoti Ranjan Panda[1], Sudhakar Sahu[1] and S Raghavan[2]

[1]School of Electronics Engineering, KIIT Deemed to be University, Bhubaneswar, India
[2]Department of Electronics and Communication Engineering, NIT Tiruchirappalli, India

Corresponding author: Satyadeep Das (satya626auro@gmail.com)

ABSTRACT An arrangement of orthogonally aligned antennas over two planes of a substrate is designed in this paper. The design is a novel miniaturized cognitive model operating at Long Term Evolution (LTE), C-band and X-band with sufficient band stop notch. The antenna is etched over a 0.8 mm thick FR-4 Epoxy substrate of dimension 15 mm x 15 mm. On one side the antenna is a hexagonal slotted microstrip antenna and on the other side is a partial Co-Planar Waveguide (CPW) type hexagonal patch antenna. The top hexagonal patch antenna is a wide band from 1800 MHz to 12000 MHz. With the use of a slot on the patch creates one notch from 2240 MHz to 5090 MHz and another notch is created at 6200 MHz to 8100 MHz. Thus, the working bands comprise of LTE 1900, Wi-Fi 5G and X-band under a single polarization. Similarly, the second antenna has its first resonance at LTE 1900 and the second resonance at X-band with a polarization orthogonal to the antenna at top. Being a miniaturized antenna, the cognitive radio provides gain ranging from 2.0 dB at lower frequency to 5.4 dB at higher frequency. The isolation over the operating bands suggests non-interference between the antennas.

INDEX TERMS Multiple-Input Multiple-Output (MIMO), Slotted Dipole (SD), Dual Polarized (DP), Co-Planar Waveguide (CPW), Ultra-Wide Band (UWB)

I. INTRODUCTION

IN par with the advancement of wireless communication systems, the prime focus of research has been the high data rate and large channel capacity. The requirement of high data rate has been catered by the concept of UWB at a low cost [1] and is widely in use for short range communications and tracking [2][3]. A mobile terminal executes several wireless communications for which the design of multiple antennas in a limited space and its placement is a major challenge. Thus, a diversified technology is targeted for a MIMO configuration, effectively suppressing multipath fading and improving channel capacity. The present trend of technology has directed the researchers towards UWB-MIMO that adds-up to the data rate [4][5].

In order to obtain pattern and polarization diversity, two elements are placed perpendicular to each other either on a single plain or on both sides of the substrate [6][7]. Moreover, there is a huge requirement to miniaturize an antenna which can be achieved by fractal designs [8][9], ground loading [10][11][12], high dielectric substrate [13], etc. Eventually this leads to strong mutual coupling between elements which can degrade the antenna performance. This issue is then addressed by the use of parasitic elements[14][15][16], defected ground structures (DGS) [17][18][19][20] electromagnetic band-gap structures [21], neutralization lines [22][23], etc.

However, all the above cited papers focus on radiating elements separated by an isolating structure to overcome the interferences. This work implements a novel ideation of two cross-polarized hexagonal radiating patches of different frequency bands arranged on both sides of the substrate satisfying the UWB concept of the overall antenna and allowing to use both the antennas at any given time frame without any interference. The proposed antenna is miniaturized to 15 mm x 15 mm of FR-4 substrate involving DGS for improving the isolation between ports.

II. DESIGN METHODOLOGY FOR THE PROPOSED MIMO

The design geometry of the proposed dual-notch MIMO antenna is illustrated in Figure 1. The top radiator is a microstrip type hexagonal patch with a circular slot and defected ground as shown in Figure 1a. Whereas the bottom radiator is a semi-CPW type hexagonal radiator placed in an orthogonal orientation to the top radiator on the other side of the substrate. The substrate used is a low cost, lossy dielectric FR-4 epoxy with relative permittivity (ε_r) 4.4 of height $h = 1.6\ mm$. The detailed simulation level analysis is executed using Ansys HFSS 17.0 [24] and Table I details all the involved dimensions for the design of the proposed antenna

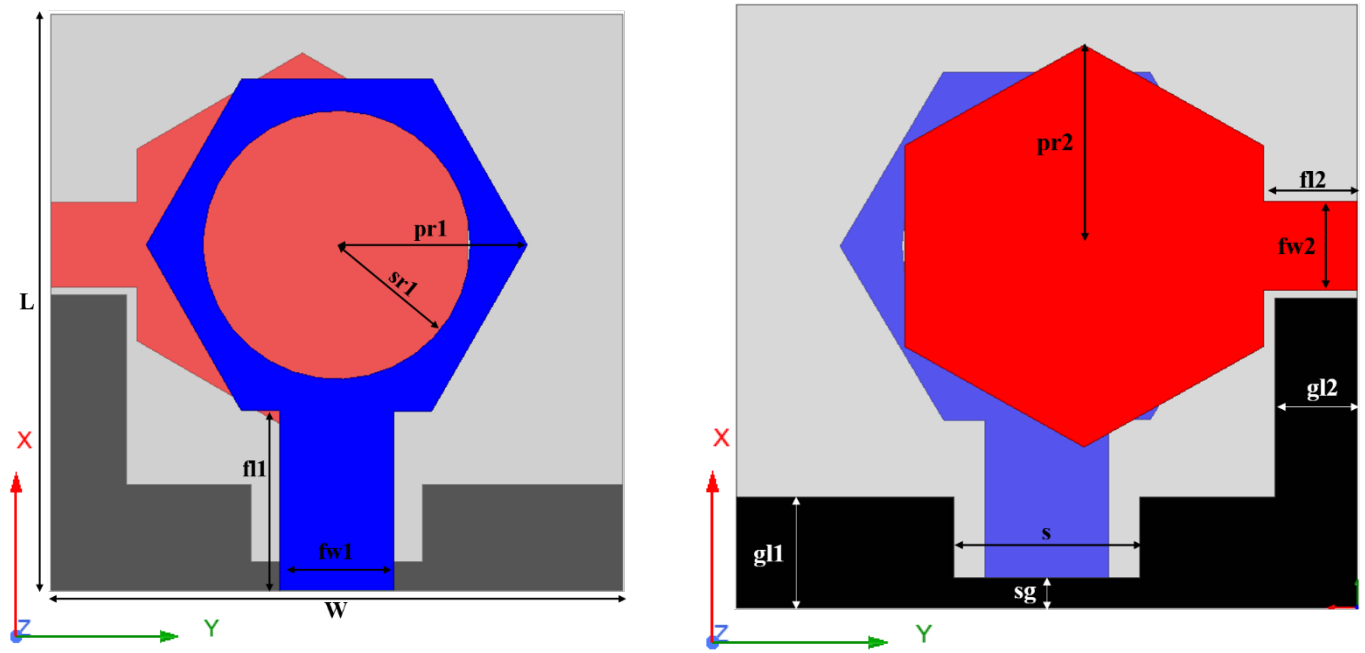

FIGURE. 1: Geometric illustration of the proposed antenna, a, Top-view, Antenna-1, b, Bottom-view, Atenna-2

TABLE I: Optimized dimensions for the proposed antenna

Symbol	Dimension (mm)	Symbol	Dimension (mm)
L	15	fl2	2.3
W	15	pr2	5
fw1	3	gl1	2.75
fl1	4.5	gl2	2
pr1	5	s	4.5
sr1	3.5	sg	0.75
fw2	2.2		

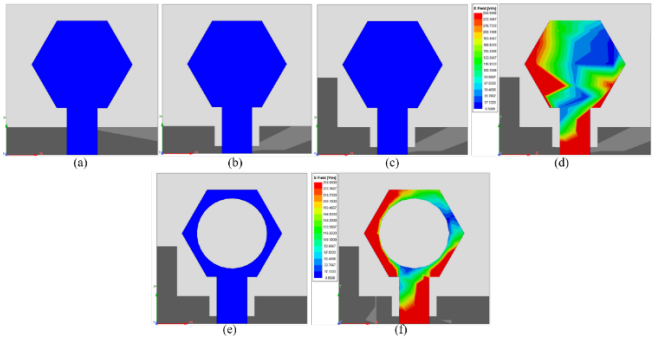

FIGURE. 2: Step-by-step evolution of top radiator and E-field analysis

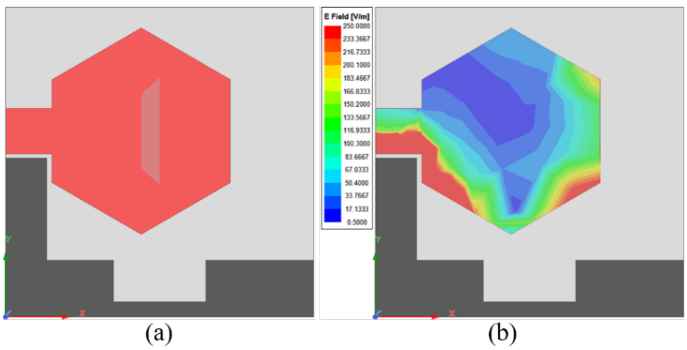

FIGURE.3: E-field analysis of the bottom radiator

A. EVOLUTION OF THE PROPOSED RADIATOR

The choice of hexagonal patch antenna for the design is definitely due to its gain enhancement and radiation pattern properties. Both the top and bottom radiators are hexagonal patches The microstrip type top hexagonal patch alone as shown in Figure 2 has dual band characteristics, LTE 1900 and X-band. The patch is fed by a feed line of width *fw1*.And the bottom patch as shown in Figure 3 is a semi-CPW type hexagonal patch with feed width *fw2*, which is mathematically calculated as Equation (1),

$$fw1, fw2 = \frac{7.48 \times h}{e^{\left(Z_0 \frac{\sqrt{\varepsilon_r + 1.41}}{87}\right)}} - 1.25 \times t \qquad (1)$$

where, t is the copper cladding of 1.6 mm over the substrate.

B. DEFINING THE ORIENTATION

In order to introduce and establish proper isolation between terminals of the radiators and also to maintain the miniature form factor and light weight, the ideas of Electro-magnetic Band Gap (EBG), neutralization line or parasitic line is not implemented. Rather the radiation polarization of the individual radiator is targeted. Two radiations from the same source with

different polarization never interfere and thus, provide port to port isolation. Hence, the top and the bottom radiators are placed orthogonal to each other. Mathematically, Equation (2), if $\vec{a}$ is orthogonal to $\vec{b}$,

$$\vec{a} \cdot \vec{b} = 0 \tag{2}$$

C. PARAMETRIC ANALYSIS

From the step-by-step evolution depicted in Figure 2, and the parametric return loss obtained in Figure 4a, we understand that the standalone hexagonal microstrip patch provides a dual band characteristic. Similarly, the bottom radiator is the standard hexagonal patch without any slot which acts as the director for the radiations of the top patch. The ground for the bottom radiator is a semi-CPW type where-in the ground plane on one side of the feed is missing. As per analysis, the ground plane on the etched-out side had no relevant effect on the radiator. This helps in less copper load on the antenna thus, adding to the light weight feature. But it covered the X-band only which is obtained by the feed width optimization. Thus, both the radiators for the proposed antenna had no operating bands between 2100 MHz to 8 GHz. After the introduction of DGS at the electric null as shown Figure 2d, and the circular slot on the top radiator, an extra matching range at C-band is also achieved from the top radiator.

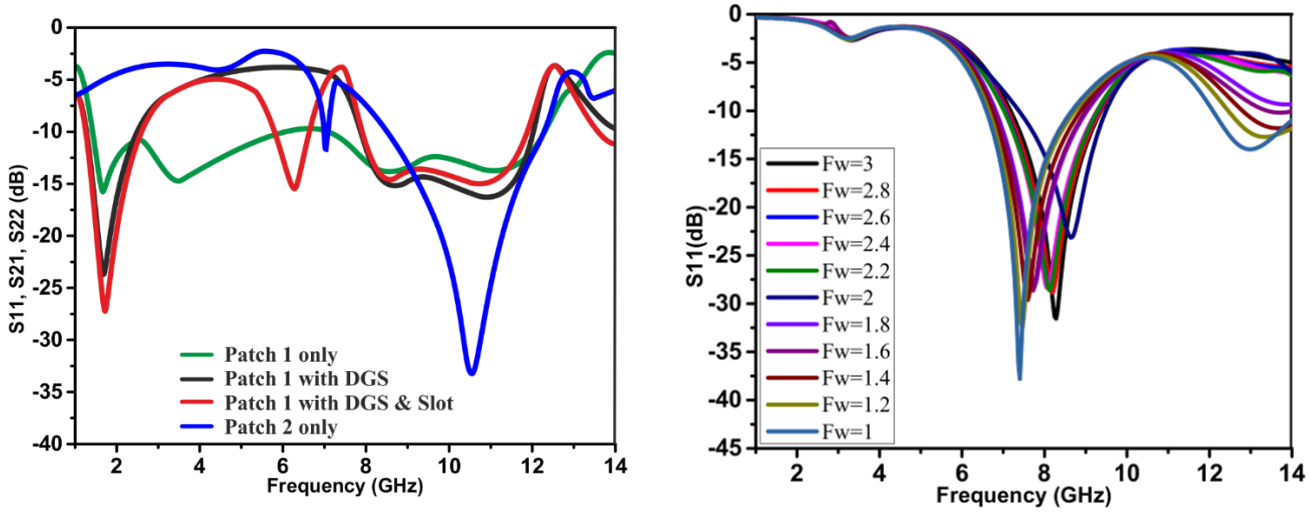

(A) (B)

FIGURE 4: Parametric analysis (A) evolution of top radiator (B) feed width optimization of bottom radiator

III. SIMULATION AND PROTOTYPE ANALYSIS

The proposed antenna is prototyped as shown in Figure 5 and is measured for the verification with the simulation results. The miniature size of the proposed antenna can be observed from the compared dimension of an Indian 5-rupee coin. The measured S-parameters as depicted in Figure 6, shows clear correlation with the simulated results for -10 dB impedance bandwidths (S11, S22) and port to port isolation (S21). As per the results, radiator 1 operates at the frequency bands 1600 MHz – 2500 MHz (LTE-1900), 5100 MHz to 6100 MHz (Wi-Fi 5G) and 7900 MHz – 12000 MHz X-band having notch at 2240 MHz to 5090 MHz and another notch at 6200 MHz to 8100 MHz. Similarly, the semi-CPW type radiator 2 without slot operates at 1700 MHz to 2100 MHz (LTE-1900) and 8400 MHz to 12000 MHz (X-band). The isolations observed between the two ports at the overlapping bands LTE-1900 and X-band, is satisfactory enough to avoid any interference.

Figure 7 picturizes the radiation pattern of the top radiator of the proposed antenna for the center frequencies 1650 MHz, 5500 MHz and 10600 MHz. The measured results give good correlation with the simulated results and the maximum variation is observed at X-band due to higher frequency where the cable used in the chamber incurs more loss.

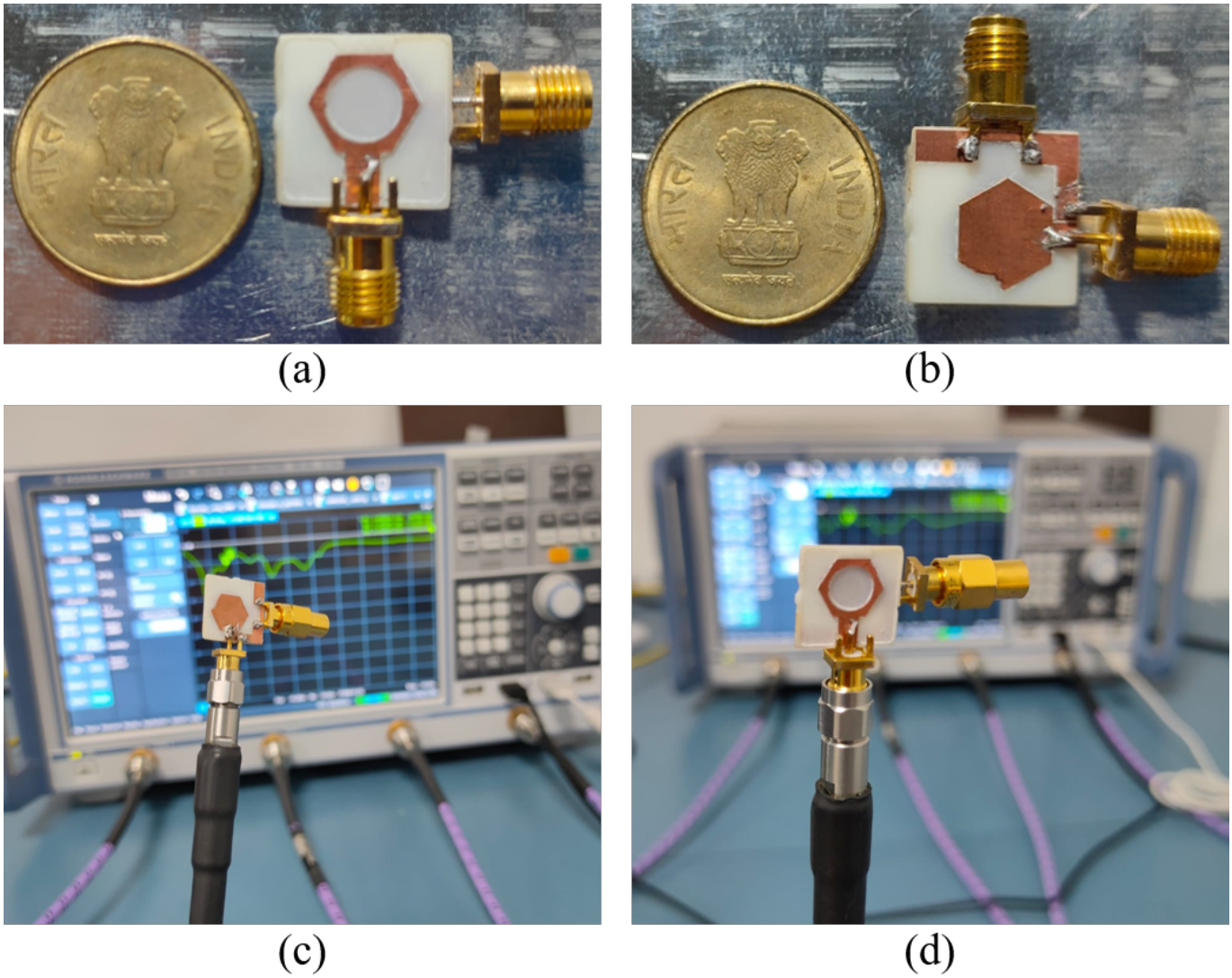

FIGURE 5: Fabricated prototype

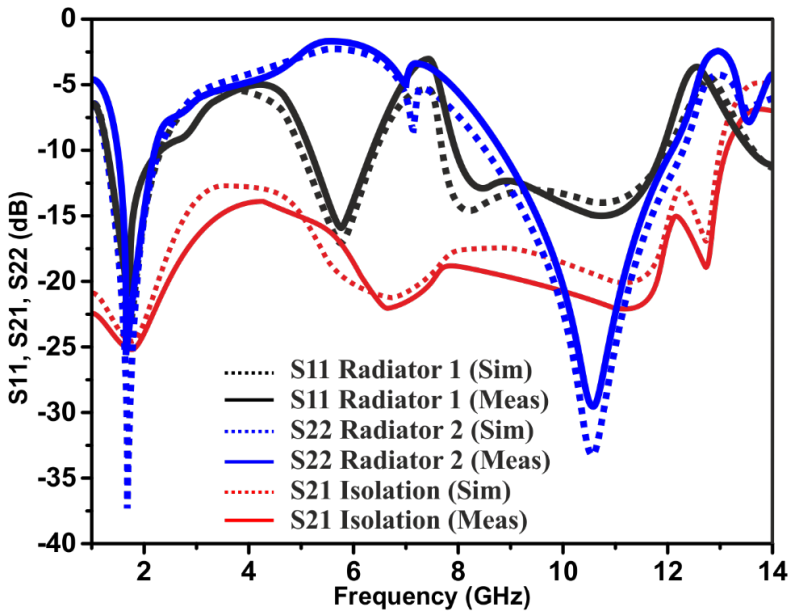

FIGURE 6: Optimized S-parameters of the proposed antenna

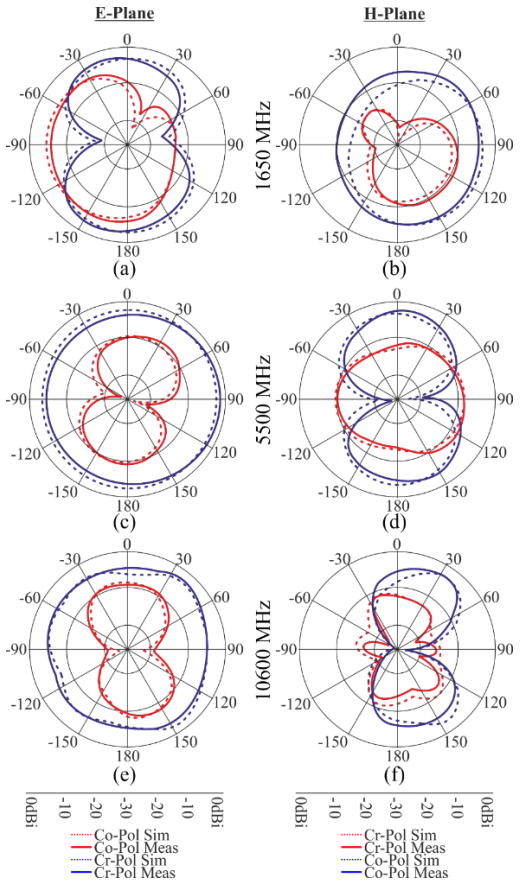

FIGURE 7: Top radiator E-plane and H-plane radiation patterns for the operating band center frequencies

Similarly, the radiation patterns for the bottom radiator in represented in Figure 8 for the center frequencies of the operating bands.

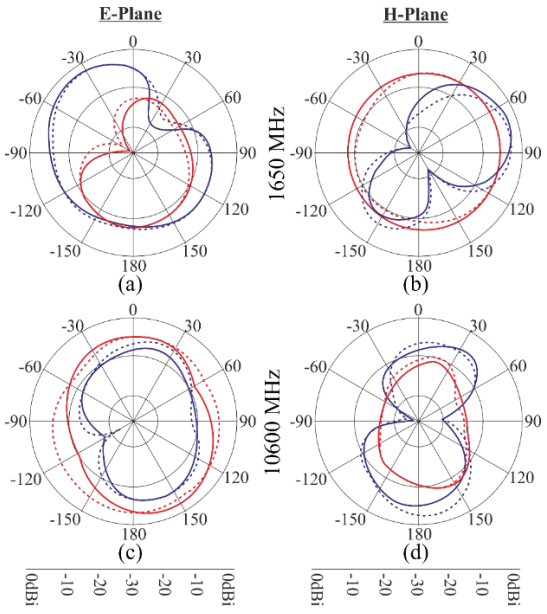

FIGURE 8: Bottom radiator E-plane and H-plane radiation patterns for the operating band center frequencies

The shift in magnitude of electric field density for the proposed antenna is presented in Figure 9.

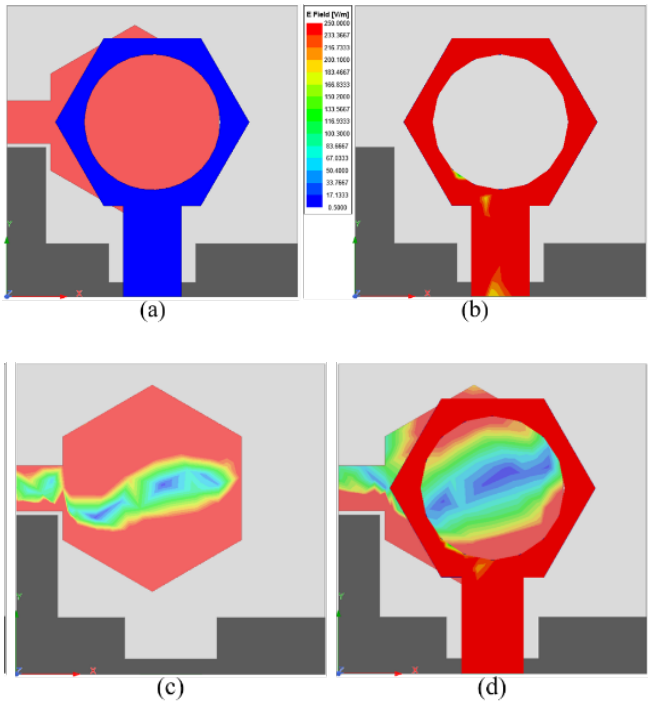

FIGURE 9: E-field impact of both radiators on each other

Thus, the electric field vectors for both the radiators for the center frequencies of the operating bands is projected in Figure 10. We can observe field vectors at the center of the bottom radiator is higher when it only acts as the reflector for bottom radiator for the C-band. For rest of the two operating bands, the bottom radiator has maximum vectors at the edges. This indicates lesser interference.

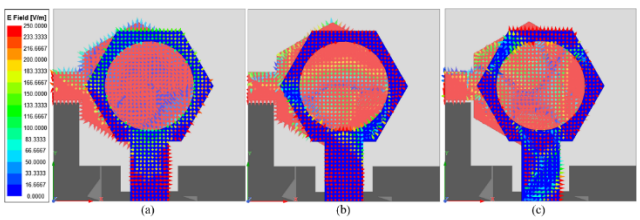

FIGURE 10: Surface current density at (a) 1.65 GHz (b) 5.5 GHz (c) 10.6 GHz

The 3D gain depicted in Figure 11 explains, as we go high on frequency, the antenna gain kept on increasing at the same time

the directivity kept on increasing the gain and decreasing the beam width. The gain for the top radiator ranges from 2.2 dB at 1.65 GHz to 4.6 dB at 10.6 GHz. Similarly, the gain of the bottom radiator ranges from 2.0 dB at 1.65 GHz to 5.4 dB at 10.6 GHz which is verified by the 2D gain plot in Figure 12.

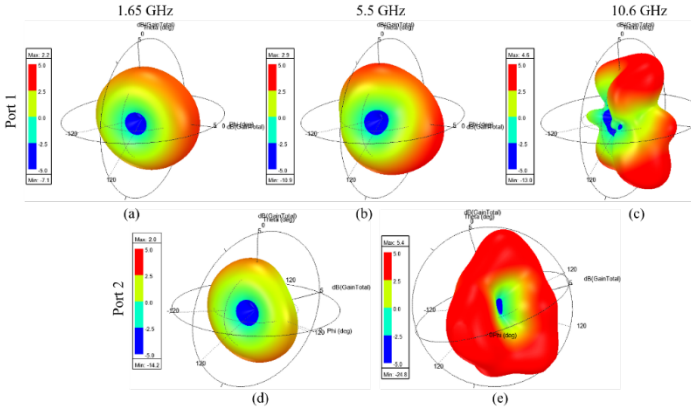

FIGURE 11: 3D Gain pattern of the proposed antenna

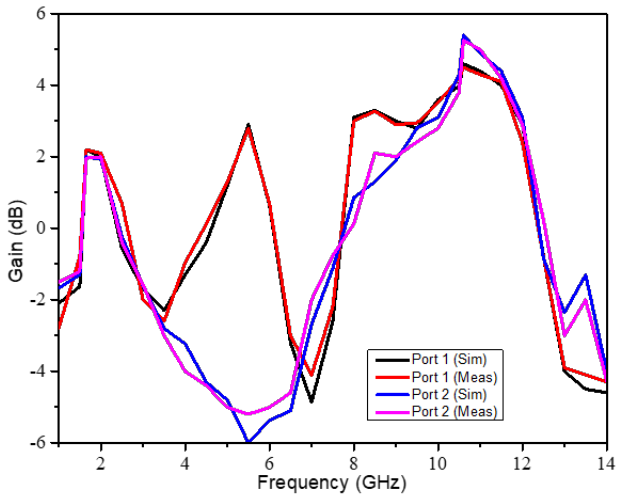

FIGURE 12: 2D Gain plot

The proposed design is verified for its cross-pol rejection (CPR) in Figure 13 that clearly explains the rejection of 6.2 dB between the orthogonal ports.

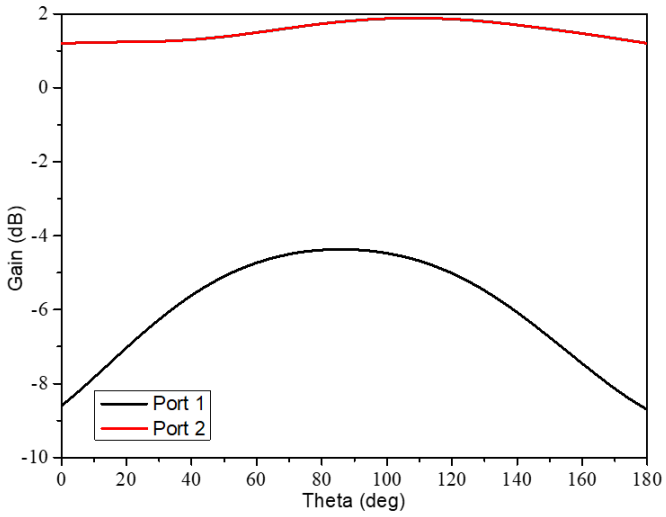

FIGURE 13: Cross-pol rejection between ports

Further, following the mathematical expressions for electro-magnetic Correlation Coefficient (ECC) and Total active reflection Coefficient (TARC) as given in eq.3&4, the graphical representation of ECC and TARC are obtained for the proposed antenna as shown in Figure 14 & 15 respectively.

$$ECC = \frac{|S_{11}^* S_{12} + S_{21}^* S_{22}|^2}{(1 - |S_{11}|^2 - |S_{21}|^2)(1 - |S_{21}|^2 - |S_{22}|^2)} \quad (3)$$

$$TARC = \sqrt{\frac{(S_{11} + S_{12})^2 + (S_{21} + S_{22})^2}{2}} \quad (4)$$

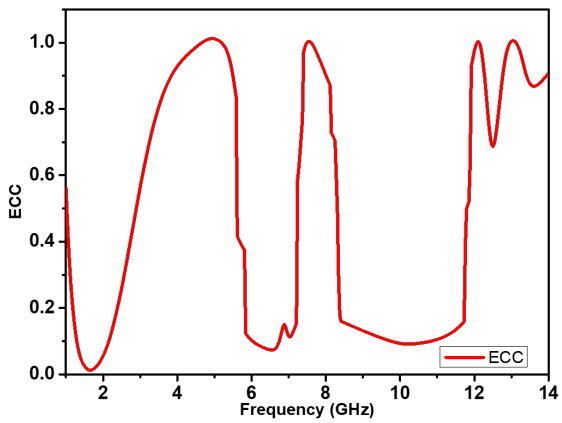

FIGURE 14: ECC of the proposed antenna

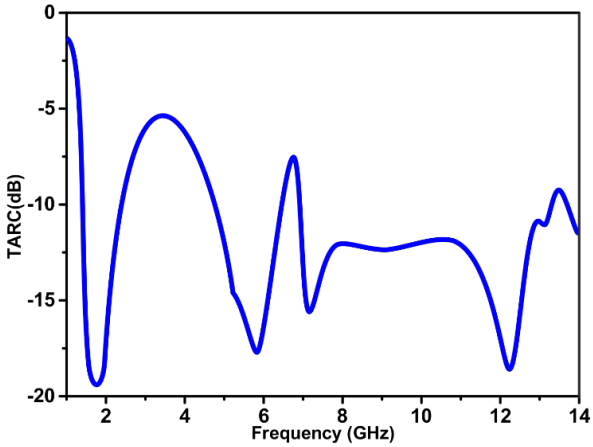

FIGURE 15: TARC of the proposed Antenna

From the graphical representations, we can observe that the ECC value is close to zero at all the three operating bands of the proposed antenna and at the same time, the TARC value for the same bands are observed to be lowest where the graph is less than 0 dB throughout.

The time domain analysis (TDM) of the proposed antenna is simulated with orientations of radiators, top-facing-top and bottom-facing-bottom. At 1650 MHz, the group delay was observed to be less than 1 ns as shown in Figure 16.

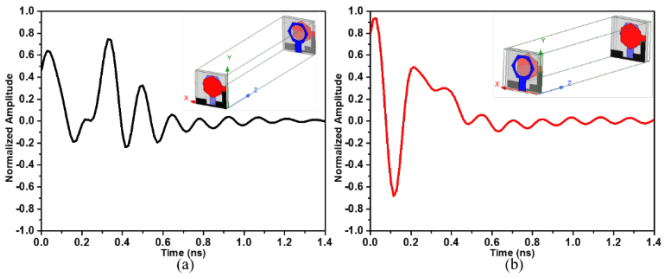

FIGURE 16: Group Delay (a) P1-P1 (b) P2-P2

IV. CONCLUSION

A 2-port cross polarized MIMO antenna system is reported in this manuscript that are designed on either side of a lossy dielectric material FR-4 epoxy. The patches used are dual band hexagonal microstrip with a slot as top radiator and semi-CPW hexagonal patch as bottom radiator. Table II shows the comparative analysis of the proposed antenna. This proposed antenna design is meant for the improvement of the channel capacity and quality of the communication link.

The top radiator gives three operational bands at 1600 MHz – 2500 MHz (LTE-1900), 5100 MHz to 6100 MHz (Wi-Fi 5G) and 7900 MHz – 12000 MHz X-band with center frequency gain of 2.2 dB, 2.9 dB and 4.6 dB respectively. Similarly, the bottom radiator operates at 1700 MHz to 2100 MHz (LTE-1900) and 8400 MHz to 12000 MHz (X-band) with center frequency gains at 2.4 dB and 5.4 dB respectively. Thus, gives the UWB in a cognitive mode of operation. The isolation obtained throughout the operating bands is also < 15 dB which is an ideal match for a cross polarized MIMO antenna for portable device applications at a unit size of 15 mm x 15 mm. This design may also be extended to triple-band (3.5/5.5/8.5 GHz) notched characteristics with 2/4 element MIMO antenna systems for low user interference and several additional architectures may be tested to further reduce mutual coupling.

TABLE II. Comparison with existing work

Ref	Antenna Size (mm)	Frequency band (GHz)	Gain (dB)	Technology
[16]	46.8 x 46.8	3.8 – 12.272	2.8 – 4.6	CPW
[18]	22 x 26	3.1 – 10.6	3.8	DGS
[20]	30 x 41	2.2 - 11	4	Hilbert Fractal
[22]	30 x 14.5	2.4	2.2	Neutralization line
[23]	21 x 34	3.52 – 9.89	3.1 – 5.12	Neutralization line
Here	15 x 15	1.6 – 12	2.0 – 5.4	Cross-Pol

REFERENCES

[1] M. G. N. Alsath and M. Kanagasabai, "Compact UWB Monopole Antenna for Automotive Communications," *IEEE Trans. Antennas Propag.*, vol. 63, no. 9, pp. 4204–4208, 2015.

[2] B. Sobhani, E. Paolini, A. Giorgetti, M. Mazzotti, and M. Chiani, "Target Tracking for UWB Multistatic Radar Sensor Networks," *IEEE J. Sel. Top. Signal Process.*, vol. 8, no. 1, pp. 125–136, 2014.

[3] T. Kaiser and B. T. Sieskul, "An Introduction to Multiple Antennas for UWB Communication and Localization," in *2006 40th Annual Conference on Information Sciences and Systems*, 2006, pp. 638–643.

[4] M. Bilal, R. Saleem, H. H. Abbasi, M. F. Shafique, and A. K. Brown, "An FSS-Based Nonplanar Quad-Element UWB-MIMO Antenna System," *IEEE Antennas Wirel. Propag. Lett.*, vol. 16, pp. 987–990, 2017.

[5] X. Zhao, S. P. Yeo, and L. C. Ong, "Planar UWB MIMO Antenna With Pattern Diversity and Isolation Improvement for Mobile Platform Based on the Theory of Characteristic Modes," *IEEE Trans. Antennas Propag.*, vol. 66, no. 1, pp. 420–425, 2018.

[6] S. Zhang, B. K. Lau, A. Sunesson, and S. He, "Closely-packed UWB MIMO/diversity antenna with different patterns and polarizations for USB dongle applications," *IEEE Trans. Antennas Propag.*, vol. 60, no. 9, pp. 4372–4380, 2012.

[7] P. Gao, S. He, X. Wei, Z. Xu, N. Wang, and Y. Zheng, "Compact printed UWB diversity slot antenna with 5.5-GHz band-notched characteristics," *IEEE Antennas Wirel. Propag. Lett.*, vol. 13, pp. 376–379, 2014.

[8] J. Pourahmadazar, C. Ghobadi, and J. Nourinia, "Novel Modified Pythagorean Tree Fractal Monopole Antennas for UWB Applications," *IEEE Antennas Wirel. Propag. Lett.*, vol. 10, pp. 484–487, 2011.

[9] A. Azari, A. Ismail, A. Sali, and F. Hashim, "A New Super Wideband Fractal Monopole-Dielectric Resonator Antenna," *IEEE Antennas Wirel. Propag. Lett.*, vol. 12, pp. 1014–1016, 2013.

[10] S. Das and S. Sahu, "Square Fractal Ring Loaded CPW-Fed Circular Polarized Antenna," in *2016 IEEE Region 10 Conference (TENCON)*, 2016, pp. 1559–1562.

[11] S. Das, A. Gupta, and S. Sahu, "Metamaterial Based Fractal-Ground Loaded Frequency-Reconfigurable Monopole-Antenna with Gain-Bandwidth Enhancement," *AEU - Int. J. Electron. Commun.*, p. 153593, Jan. 2021.

[12] Z. Chen, W. Zhou, and J. Hong, "A Miniaturized MIMO Antenna with Triple Band-Notched Characteristics for UWB Applications," *IEEE Access*, vol. 9, pp. 63646–63655, 2021.

[13] S. Chen, G. Liu, X. Chen, T. Lin, X. Liu, and Z. Duan, "Compact Dual-Band GPS Microstrip Antenna Using Multilayer LTCC Substrate," *IEEE Antennas Wirel. Propag. Lett.*, vol. 9, pp. 421–423, 2010.

[14] A. Iqbal, O. A. Saraereh, A. W. Ahmad, and S. Bashir, "Mutual Coupling Reduction Using F-Shaped Stubs in UWB-MIMO Antenna," *IEEE Access*, vol. 6, pp. 2755–2759, 2018.

[15] M. A. Ul Haq and S. Koziel, "Ground Plane Alterations for Design of High-Isolation Compact Wideband MIMO Antenna," *IEEE Access*, vol. 6, pp. 48978–48983, 2018.

[16] F. Urimubenshi, D. B. O. Konditi, and E. N. Ndung'u, "Design of a compact two-port MIMO antenna for UWB applications," *Int. J. Sci. Technol. Res.*, vol. 8, no. 12, pp. 1856–1860, 2019.

[17] H. T. Chattha, M. Nasir, Q. H. Abbasi, Y. Huang, and S. S. Alja'Afreh, "Compact low-profile dual-port single wideband planar inverted-F MIMO Antenna," *IEEE Antennas Wirel. Propag. Lett.*, vol. 12, pp. 1673–1675, 2013.

[18] C. Luo, J. Hong, and L. Zhong, "Isolation Enhancement of a Very Compact UWB-MIMO Slot Antenna With Two Defected Ground Structures," vol. 14, pp. 1766–1769, 2015.

[19] A. Gorai and R. Ghatak, "Utilization of Shorted Fractal Resonator topology for high isolation and ELC resonator for band suppression in compact MIMO UWB antenna," *AEU - Int. J. Electron. Commun.*, vol. 113, p. 152978, 2020.

[20] A. Gorai, A. Dasgupta, and R. Ghatak, "A compact quasi-self-complementary dual band notched UWB MIMO antenna with enhanced isolation using Hilbert fractal slot," *AEU - Int. J. Electron. Commun.*, vol. 94, pp. 36–41, 2018.

[21] X. Yang, Y. Liu, Y. X. Xu, and S. X. Gong, "Isolation enhancement in patch antenna array with fractal uc-ebg structure and cross slot," *IEEE Antennas Wirel. Propag. Lett.*, vol. 16, pp. 2175–2178, 2017.

[22] S. Su, C. Lee, and F. Chang, "Printed MIMO-Antenna System Using Neutralization-Line Technique for Wireless USB-Dongle Applications," vol. 60, no. 2, pp. 456–463, 2012.

[23] R. N. Tiwari, P. Singh, and B. K. Kanaujia, "A compact UWB MIMO antenna with neutralization line for WLAN/ISM/mobile applications," *Int. J. RF Microw. Comput. Eng.*, vol. 29, no. 11, pp. 1–9, 2019.

[24] Ansys, "HFSS v17.0." .